metals

MDPI

Article

An X-ray Microscopy Study of the Microstructural Effects on Thermal Conductivity in Cast Aluminum-Copper Compounds

Andreas Christopher Fromm, Christoph Kahra, Armin Selmanovic, Hans Jürgen Maier and Christian Klose *

Institut für Werkstoffkunde (Materials Science), Leibniz Universität Hannover, 30823 Garbsen, Germany; fromm@iw.uni-hannover.de (A.C.F.)
* Correspondence: klose@iw.uni-hannover.de

Abstract: A metallurgical joint between aluminum and copper established by compound casting provides for high thermal conductivity, which is required for lightweight cooling solutions in applications such as high-power light-emitting diodes or computer processors. If casting is employed in a silane-doped inert gas atmosphere whose oxygen partial pressure is adequate to extreme high vacuum, reoxidation of the active surfaces of aluminum and copper is prevented, and thus a metallurgical bond can be created directly between aluminum and copper. With this approach, thermal conductivities as high as 88.3 W/m·K were realized. In addition, X-ray microscopy was used to shed light on the microstructure–thermal property relationship. It is demonstrated that both porosity and non-bonded areas have a substantial impact on the thermophysical properties of the compound zone. Based on the data obtained, casting parameters can be developed that provide for defect-free bonding zones and optimal heat transfer between the joining partners.

Keywords: aluminum-copper compounds; compound casting; silane; microstructure; thermal conductivity; X-ray microscopy; volumetric characterization; Kirkendall effect; porosity

Citation: Fromm, A.C.; Kahra, C.; Selmanovic, A.; Maier, H.J.; Klose, C. An X-ray Microscopy Study of the Microstructural Effects on Thermal Conductivity in Cast Aluminum-Copper Compounds. *Metals* **2023**, *13*, 671. https://doi.org/10.3390/met13040671

Academic Editor: Jose Miguel Molina Jordá

Received: 28 February 2023
Revised: 24 March 2023
Accepted: 27 March 2023
Published: 29 March 2023

1. Introduction

Due to the excellent thermal conductivity of copper, it is often used for heat sinks in order to dissipate the heat generated by modern electronic devices with high power densities. To reduce the required amount of copper, a compound of aluminum and copper is often used, which helps to reduce total costs. In addition, aluminum has lower density and higher specific heat capacity, which makes it an excellent joining partner for copper in this application. However, the interface between the joint metals is critical in terms of thermal resistance. Different joining techniques are used, e.g., in microelectronics, medical applications, optoelectronics, and microsystems [1]. Mass-manufactured copper-aluminum compounds for heat sinks that are mechanically joined often have an air-filled gap between the joining partners, which has a very low thermal conductivity (λ_{air} = 0.03 W/m·K) and thus waste potential for highly efficient cooling solutions. Thus, compound casting that can potentially overcome limitations such as sample size or high manufacturing costs [2] was chosen in this study to improve thermal conductivity. However, the native oxide layers normally present on both the copper and the aluminum prevent the two metals from bonding during casting because the oxide layer acts as diffusion barriers [2]. Thus, in an earlier study, a zinc-based layer, which acted as a low-melting bonding agent, was applied on top of a copper insert prior to high pressure die casting of an aluminum-copper compound [3]. With this approach, the thermal conductivity between the two joining partners could be increased to >100 W/m·K. However, this imposes limits on the process as it is challenging to realize an even zinc coating on challenging geometries.

Other studies have also achieved very good results using coatings [4–6] or a near-net forming process [7]. For instance, it could be shown that the formation of the brittle and hard Al-Mg intermetallic compounds could be suppressed using a Ni-Cu composite interlayer along with a simultaneous increase in shear strength by more than 20% [5].

In similar studies, increased thermal conductivity and improved mechanical properties have been achieved by dispersing silicon wiskers in a magnesium melt, which are then bonded to copper layers by warm accumulative roll bonding (ARB) [8]. The same effect was observed with silicon particles sandwiched between aluminum and nickel layers bonded to copper plates from the outside using the ARB process [9]. In both studies, different rolling process cycles led to a reduction in thermal conductivity. However, by combining the cold roll bonding (CRB) and ARB processes, Al/Cu functionally graded metal matrix composites could be produced, which also showed an increase in thermal conductivity [10] and in strength [11].

Recently, it was demonstrated that compound casting in an oxygen-free environment is another alternative that does not rely on the use of low-melting intermediate layers [12]. Instead, the oxide layers are removed by mechanical grinding, and the oxygen-free environment prevents re-formation of the interfering oxides. Such an atmosphere can be created by the addition of silane (SiH_4) to an inert gas such as argon 5.0.

In a compound casting between copper and aluminum three layers form, i.e., an eutectic structure of α-aluminum and Al_2Cu, a layer of Al_2Cu, and an intermetallic phase seam. The formation of the phase seam is controlled by copper diffusion as shown by experiments [13] and simulations [14]. Tayyebi et al. [15] combined pure copper and Al5052 sheets using the ARB process via several annealed rolling processes and produced intermetallic phases such as Al_2Cu or Al_4Cu_9 between the materials. These resulted in an increase in tensile strength. Additionally, casting defects such as pores and non-bonded areas can occur depending on the temperature-time regime applied during solidification and shrinkage. Since the pores in a casting are often the main cause of failure [16], there size, volume fraction and spatial distribution needs to be controlled. For measurement of these parameters computed tomography (CT) or µCT are regularly used. In case of small samples, X-ray microscopy (XRM) provides for even higher spatial resolution. In order to determine the overall influence of the compound zone properties on thermal resistance, it is necessary to characterize not only the developing phases within the compound zone, but also the size of the well-bonded areas and the volume and size distribution of the pores. Whereas conventional two-dimensional analyses based on metallographic sections probe only one plane of the sample, volumetric methods such as XRM provide for a three-dimensional image of the compound zone. It is even possible to detect the directional solidification of aluminum alloys in situ with respect to porosity formation [17]. Porosity is often evaluated in terms of pore size, the number of pores, the spatial distribution of pores along the height, and a distinction between open and closed pores can be made [18]. In the case of gas pores, a single contiguous region is usually present. However, 2D images based on metallographic sections may show an individual pore in form of isolate adjacent pores, and thus often underestimate the maximum pore size. With XRM, such contiguous pores can be better identified in the 3D images [19]. Nourian-Avval et al. [20] have also shown that pores in metallographic microsections often appear smaller than in µCT scans. Moreover, the data obtained from metallographic sections depend on the position of the random cross section, and thus often miss the largest pore, which can be critical both in terms of mechanical properties and in terms of thermal properties.

Since two materials are joined with heat in this study, the different volume change in the metals and the associated Kirkendall effect [21] must be taken into account. While this effect is useful in the production of hollow nanostructures [22,23], it leads to porosity and a loss of adhesion strength between the compound, which is why this effect is perceived as disturbing during soldering [24] and casting [25]. Another issue is shrinkage porosity. For instance, Mathew et al. [26] report the formation of shrinkage porosity in casting experiments of an AlSi7 alloy caused by incomplete melt flow during solidification. By increasing the superheating temperature of the melt, silicon particles could be reincorporated, but the porosity detected by X-ray computed tomography of the alloys increased. In essence, the different types of pores need to be accurately characterized in order to be able to improve compound casting processes.

In the present study, XRM scans were performed on aluminum-copper samples, which were manufactured by compound casting in an oxide-free atmosphere, to determine the volume of imperfections inside the compound zone such as pores and non-bonded areas between the joining partners. Taking the layered composition of the compound zone into account, the influence of the imperfections on the thermal conductivity was investigated. However, the large differences in density and atomic number between copper and aluminum pose a major challenge for the XRM analyses, i.e., it is difficult to obtain a clear image of the compound zone. A case in point are beam hardening artifacts, which can lead to overestimation of the material thicknesses, or render low-density areas such as aluminum and hollow spaces almost invisible. Thus, the objective of this study was to obtain high-fidelity volumetric scans that allow for the determination of the pore volume and discriminate between pores and non-bonded areas.

2. Materials and Methods

2.1. Compound Casting

Compound casting experiments and sample preparation were performed according to an earlier study [12]. Copper discs with a diameter of 31.8 mm were cut by electrical discharge machining from a 2 mm thick cold-rolled oxygen-free highly conductive copper plate (Hans-Erich Gemmel & Co. GmbH, Berlin, Germany) with >99.65% purity. These cylindrical copper inserts were cleaned with ethanol prior to the compound casting experiments. For casting, aluminum with a purity of >99.87% (Hydro Aluminum High Purity GmbH, Grevenbroich, Germany) was heated to 200 °C to remove water residues.

The casting tests (Figure 1) were carried out inside a glovebox (Labmaster 130, Mbraun GmbH, Munich, Germany) in an atmosphere that was adequate to extreme high vacuum in terms of the oxygen partial pressure. Specifically, the residual oxygen of the inert gas atmosphere was reduced to $<10^{-17}$ vol.-% with the aid of silane-doped argon (1 vol.-% SiH_4 in Ar 5.0–99.999% purity). The oxygen content was continuously monitored by means of a λ-probe. The oxide layers of the copper disks were removed inside the glovebox using abrasive paper. Due to the absence of oxygen, reformation of the native oxide layer was inhibited. The de-oxidized copper plate was placed in a boron nitride-coated steel mold with a cylindrical cavity (Ø 32 mm), which was then pre-heated using heating cartridges. In the casting experiments, the mold temperature was varied between 350 and 500 °C in intervals of 50 °C. The temperature of the copper insert was measured with a type-K surface thermocouple directly before casting.

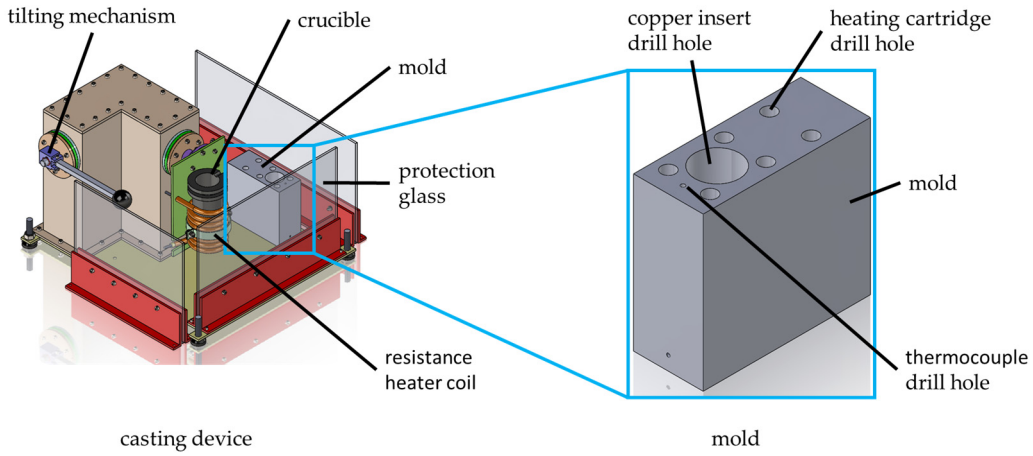

Figure 1. Schematic of the oxygen-free glovebox and the casting device including the mold.

The pure aluminum ingots were heated inside the crucible to temperatures between 750 and 800 °C (25 °C steps) by a resistance heater coil. Using different temperature regimes, 14 casting experiments were carried out. The liquid aluminum was poured in the mold onto the copper insert to create a bond between the two metals. After the specimens

were cooled to room temperature, the compound casting samples were ejected from the glovebox and shortened by turning until the copper part had a plane-parallel thickness of 1 mm ± 0.1 mm and then turned to a total thickness of 3 mm. By wire erosion, samples of 8 mm diameter each were taken from the compounds for the analyses of the compound zone properties.

2.2. X-ray Tomography—Volumetric Evaluation of Porosity

To determine the porosity and the quality of the bonding between the joining partners, XRM was employed. Using a flat panel detector, the tomographies were created with a Zeiss Xradia 520 Versa (Carl Zeiss AG, Oberkochen, Germany) X-ray microscope. At an accelerating voltage of 160 keV and an exposure time of 0.12 s, 1601 projections were acquired per sample. The spatial voxel size was 6.6 µm × 6.6 µm × 6.6 µm. To obtain the tomographies, the cylindrical samples were placed in the beam path and rotated. During this procedure, projections (two-dimensional images) were recorded at different angles. The tomography was then reconstructed from the projections after the measurement. If the joining zone was placed parallel to the X-ray beam path, the high density of the copper (8.96 g/cm^3) and the orientation of the edges of the bonded parts resulted in visual artifacts in the tomographies (Figure 2a). Even at maximum acceleration voltage of the X-ray source, it was not possible to penetrate the copper part (diameter of 8 mm) sufficiently. Particularly at the edges in the bonding zone, strong artifacts occurred in the images caused by attenuation of the X-rays due to their long path through the dense materials. To counteract this, the samples were tilted by 10° (Figure 2b). Hence, the path of the X-rays through the copper was reduced and the X-rays no longer directly hit the edges in the joining zone. As a result, the joining zone was nearly free of artefacts, which enabled quantitative analysis of the material distribution based on the different contrasts.

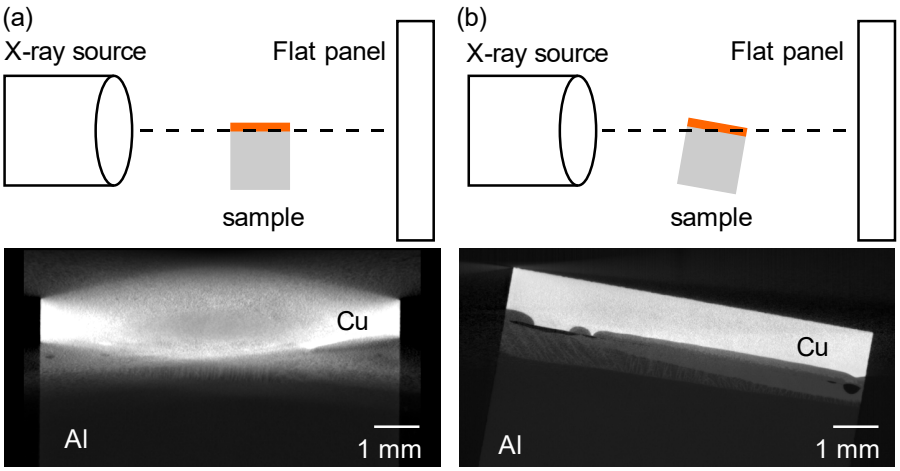

Figure 2. Schematic of the sample orientation in the beam path and change in artefacts in cross-sections from the tomographies: (**a**) parallel, (**b**) tilted by 10° to the beam direction.

The software Dragonfly 2020 (ORS, Montréal, QC, Canada) was used to reconstruct the tomography and create the images. Due to the large contrast difference between aluminum and copper, caused by the large differences in atomic number and density, the gray values of the aluminum part appeared in a similar range as the surrounding air. Hence, it was difficult to isolate the pores using the gray value differences between the air in the pores and the surrounding material when considering the measured volume in total. By dividing the regions of interest into a low to medium and a medium to high contrast range for the analysis, it was possible to determine the contours of the pores and the bonding defects. The threshold gray values were chosen such that either the copper and the side of the compound zone facing the copper or the aluminum and the side of the joining zone facing the aluminum could be evaluated. The volumes of the isolated pores

and bonding defects were then combined into a total volume that was used to determine the overall porosity and bonding quality. Porosity was determined as the ratio of the pore volume to the total volume of the material, as used in other studies [18,27,28]. With these data, it was possible to measure the compound zone thickness (CZT) three-dimensionally. Subsequently, the volume data of the compound zone was correlated with the thermal conductivity measurements obtained for these specimens.

2.3. Thermal Conductivity Measurement

The wire-eroded samples from the Al-Cu compounds (diameter 8 mm and thickness 3 mm) were also used to determine their thermal conductivity. First, the samples were coated on both sides with a thin graphite layer and then irradiated using a xenon flash (LFA 447 from Netzsch-Gerätebau GmbH, Selb, Germany). An indium antimonide infrared detector recorded the temperature change on the opposite side, from which the thermal diffusivity a was then calculated. With the density ρ, determined using an MK 2000 density measuring scale (MK Industrie-Vertretungen GmbH, Stahlhofen am Wiesensee, Germany) and the specific heat capacity c_p of the material, the thermal conductivity λ was calculated using:

$$\lambda = a \cdot c_p \cdot \rho \tag{1}$$

The thermophysical properties were first determined for the bulk materials, copper and aluminum. Next, the properties of the compound zone between the two materials were evaluated. For this purpose, the samples were approximated as a three-layer system with the compound zone acting as the contact resistance R in between aluminum and copper. For evaluation of thermal conductivity, the individual compound zone thickness of each sample is a critical parameter. Thus, the thickness of the compound zone was determined from the three-dimensional analyses described in Section 2.2. With these data, the thermal conductivities λ_{CZT} can be calculated as [29]:

$$\lambda_{CZT} = \frac{CZT}{R} \tag{2}$$

The thermal conductivities were measured between 25 °C and 200 °C. As thermal conductivity was found to depend only slightly on temperature, the value at 25 °C is given in the following.

3. Results

3.1. Compound Zone Thickness

In an earlier study [12], it was shown that compound casting in an oxygen-free environment does not affect the type of phases formed. As seen in Figure 3, starting from aluminum, the compound zone consists of an eutectic structure formed by an α-aluminum (α-Al) solid solution and the θ-phase (Al_2Cu), followed by a layer of the θ-phase, and finally an intermetallic layer of the η_2-phase (AlCu) and γ-phase (Al_4Cu_9).

The corresponding EDX line scans shown in Figure 4 demonstrate the chemical composition of the different phases. Based on their stoichiometric compositions, the phases close to the copper insert can be assumed to be of the Al_4Cu_9 and AlCu type.

As described earlier, it was possible to display the compound zone three-dimensionally over several slices by adjusting the X-ray energy and the positioning of the specimens. In Figure 5, copper is displayed in light gray, whereas the aluminum is dark gray with the compound zone in between. In addition, casting-related pores are visible, which appear black. With this set-up and contrast setting, it was possible to measure the compound zone thickness slice by slice to determine the variation in thickness across the specimen. As an example, Figure 5 shows three representative images along with the CZT measured at three locations each.

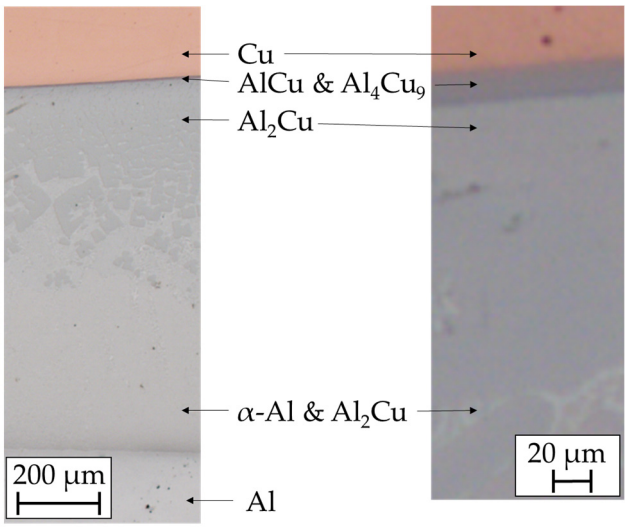

Figure 3. Example of a microscopic image of a polished composite casting sample.

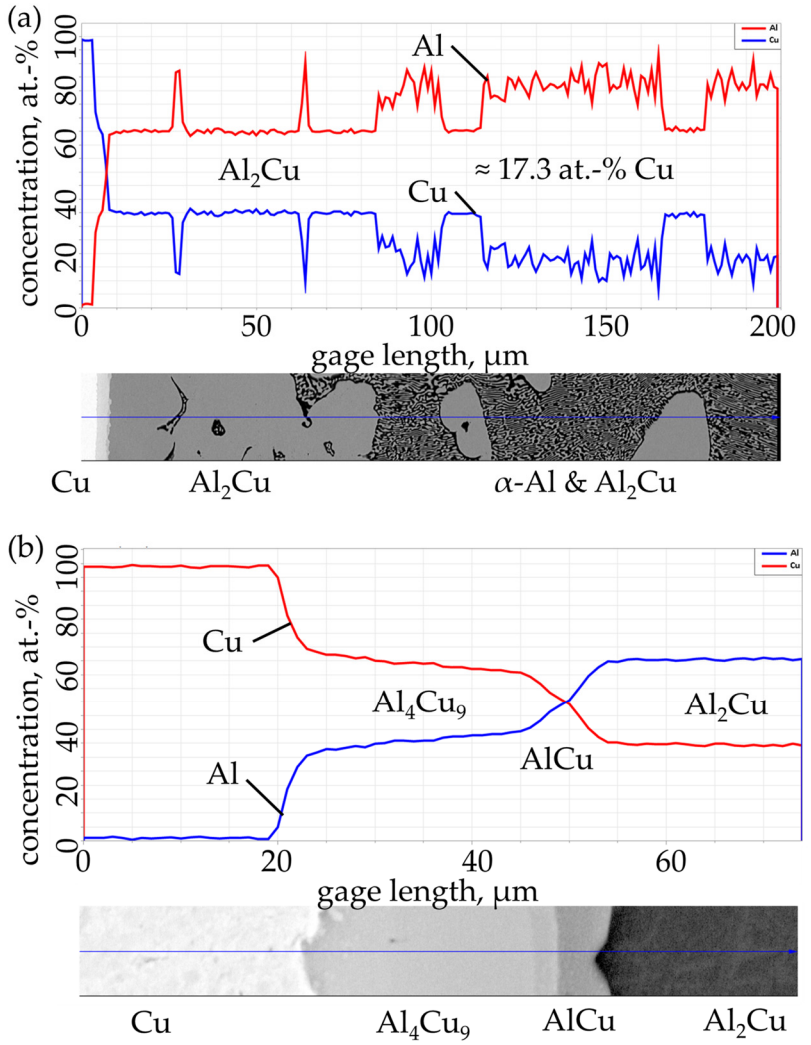

Figure 4. Representative SEM images and corresponding EDX line scans of a cast sample: (**a**) overview covering the region from Cu to α-Al, (**b**) higher magnification detail focusing on the phases present close to the Cu insert.

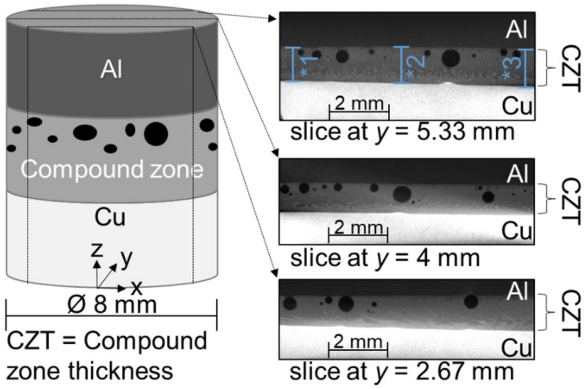

Slice at y = 5.33 mm	CZT, mm
X = 1 mm (*1)	0.85
X = 4 mm (*2)	0.9
X = 7 mm (*3)	0.94
CZT slice mean $\frac{*1+*2+*3}{3}$	0.897
CZT sample mean for 5 slices at y = 1.33 mm, 2.67 mm, 4.00 mm, 5.33 mm, 6.67 mm	0.896 ± 0.043

Figure 5. Example of a slice-by-slice measurement of the compound zone thickness along the *y*-axis, for the slice at y = 5.33 mm the measurement is shown in blue for three measuring points (sample casting parameters: aluminum temperature 713 °C, copper temperature 402 °C).

Figure 6 shows the mean CZT, determined on five different slices (y = 1.33 mm, 2.67 mm, 4.00 mm, 5.33 mm, and 6.67 mm) per specimen, for three different casting conditions. Clearly, there is a substantial variation of the thickness of the compound zone along the cross-section of the sample, which is especially evident for the specimen marked in blue. These variations are attributed to thermal fluctuations during solidification. From the data, it is also obvious that conventional single-plane measurements of the compound zone thickness can be misleading. Since the thermal properties of the compound zone are measured integrally, the volumetric imaging is particularly important to determine a meaningful average, which is required to establish a sounder correlation of the compound zone properties with the actual microstructure and processing conditions.

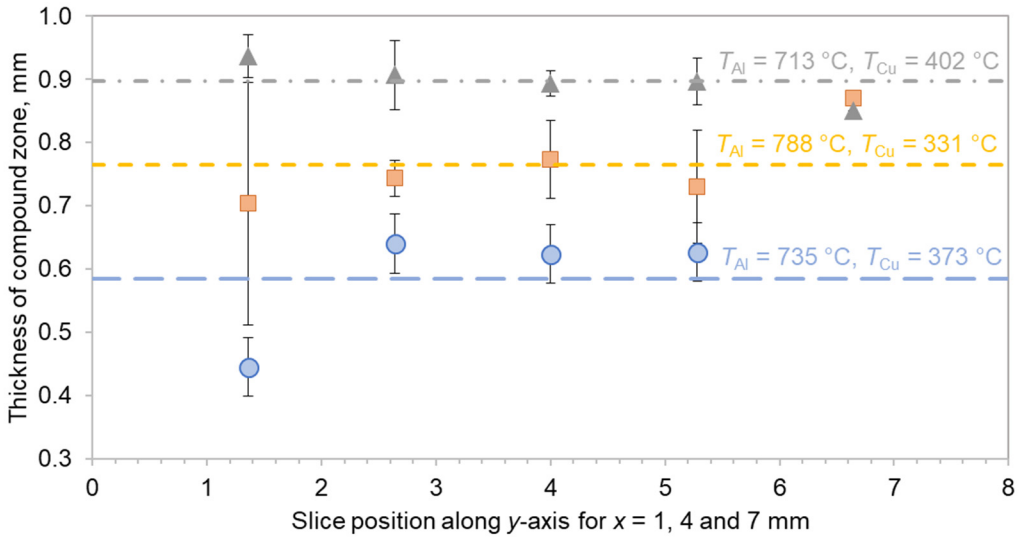

Figure 6. Compound zone thicknesses of three different specimens, measured at different positions along the *y*-axis (for the coordinate system used, see Figure 5).

Figure 7 further illustrates the need for accurate volumetric data to draw sound conclusions about the thermal conductivity–microstructure–process relationship. At first glance, a rather weak correlation seems to present between the copper insert temperature and the CZT. However, pores and non-bonded areas, which have a significant influence on the thermophysical properties, are not considered in this diagram. As shown in the following, it is crucial to determine both the volume and the distribution of the pores, and the presence of non-bonded areas based on the three-dimensional scans in order to understand their effect on the apparent thermal resistance of the compound zone.

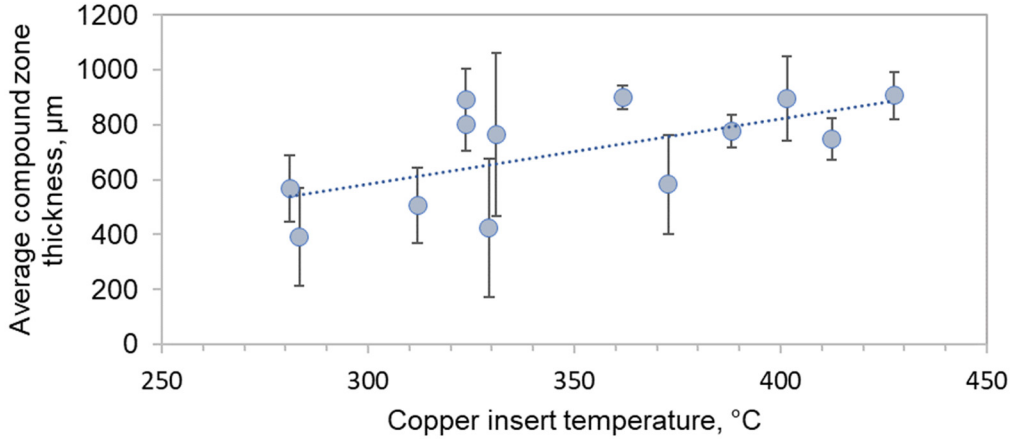

Figure 7. Average of the compound zone thickness depending on the copper insert temperature during casting.

3.2. Porosity and Bonding Areas

As described in Section 2.2, it was possible to separate the pores and the non-bonded areas in the images recorded by XRM despite the small difference in their contrast based on a threshold approach to compensate for the stark difference between copper and the less-dense materials. As shown in Figure 8 the top and the bottom parts of the pores could then be clearly identified. After setting the suitable gray values, the two halves of the images were merged to also reveal the non-bonded areas between copper and aluminum (marked in blue in Figure 8a). All defects, i.e., pores as well as non-bonded areas, were then combined to calculate the apparent porosity percentage for the compound zone.

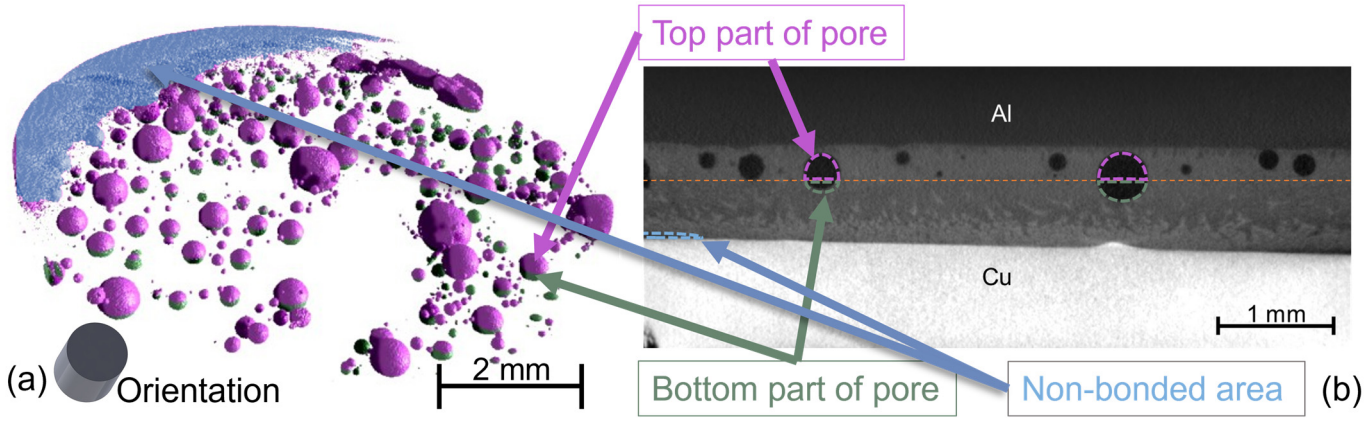

Figure 8. Compound image: (**a**) Defect volume in the whole sample with high porosity and non-bonded areas, (**b**) 2D XRM image of the same sample at y = 5.33 mm showing porosity and non-bonded area.

The thermal resistances of the compound zones of all samples were measured as described in Section 2.3. Using the CZT, the thermal conductivity was then calculated as defined in Equation (2). Next, the thermal conductivity of each specimen was correlated with the apparent porosity (Figure 9). Based on the volumetric scans, all samples were classified into non-bonded (red), partially bonded (orange), or well-bonded (green) (Figure 9a). Figure 9b shows a sample that is well-bonded despite the large number of spherical pores. The sample in Figure 9d shows a non-bonded sample whose interface had very low mechanical strength. All areas of the compound zone that were not bonded form a barrier for heat dissipation in the compound zone. In Figure 9c, a partially bonded specimen is shown. Although contrast is less than ideal in this case, the non-bonded area is obvious on the left-hand side while the rest appears to be well-bonded with few pores.

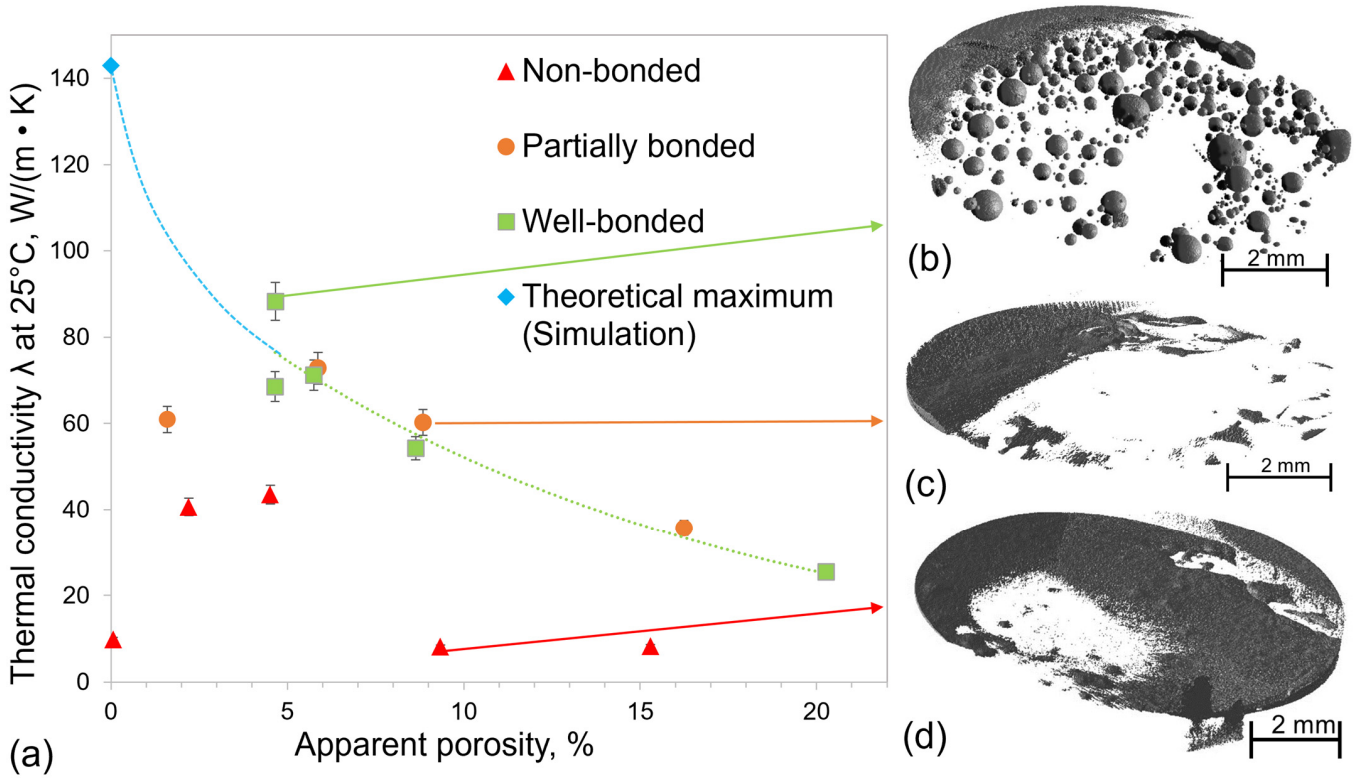

Figure 9. (**a**) Measured thermal conductivity of the compound zone for different apparent porosities, (**b**) representative samples which were considered as well-bonded, (**c**) partially bonded and (**d**) non-bonded; the maximum thermal conductivity for the compounds was taken from Ref. [29].

If all data shown in Figure 9 are considered, there seems to be no clear correlation between thermal conductivity and apparent porosity. To discriminate between the effects of the pores and non-bonded areas, only specimens that were well-bonded were then considered for the correlation between thermal conductivity and porosity. These data then show the expected strong dependence of thermal conductivity of the compound zone on porosity.

In a related study [30], the thermal conductivity of the compound zone was simulated. A maximum value of 143 W/m·K was calculated for the ideal case where there are no pores and there is a full interface-wide bond present. As shown in Figure 7, the CZT increases with increasing casting temperature. Since this leads to a decrease in thermal conductivity, the CZT must be kept as thin as possible. In previous investigations, a minimum CZT between 470 and 630 µm was obtained at low casting temperatures [12]. In the present study, the CZT was further reduced to a value between 390 and 570 µm for a copper insert temperature of 280 °C and the thermal conductivity was increased to 88.3 W/m·K. From Figure 9 it is obvious that both porosity and non-bonded areas need to be kept to a minimum to obtain high thermal conductivity.

4. Discussion

The metals copper and aluminum were chosen because of their high individual thermal conductivities. For rapid heat transfer between the metals, e.g., for heat sink applications, a metallurgical bond such as that produced in the XHV-adequate atmosphere is of paramount importance. However, temperature fluctuations during mold filling and solidification can have an impact on the performance of the compound castings. As shown in Figure 6, the local CZT varies in different cross sections of the specimen. Thus, an average value from a single metallographic cross-section is hardly representative of the true situation. By contrast, a three-dimensional image that can be acquired by µCT or XRM scans allows for a more reliable determination of the average CZT.

However, when imaging of layers between materials with substantially different density and atomic number, strong artifacts may arise. The approach used in the present study, cf. Figures 2 and 8, allowed for a reliable, quantitative evaluation of the CZT, porosity, and non-bonded areas. Similar approaches were successfully used with other material compounds such as copper–steel and copper–aluminum [1]. In the present study, a 10° tilt was necessary because larger samples with higher thickness were used in addition to the differences in density and atomic number, leading to even stronger attenuation of the X-rays.

With increased diffusion rates at higher temperatures [31], the CZT and the formation of intermetallic phases also increases [12]. These phases are often hard and brittle, which reduces strength and ductility [1] and also the thermal conductivity at the same time [12]. If the porosity is reduced, the result is an increased thermal conductivity of the compound zone. For the present Al-Cu castings, a maximum thermal conductivity of the compound zone of 88.3 W/m·K was obtained, which is more than 3000 times that of dry air. If the theoretical maximum thermal conductivity of 143 W/m·K of such castings [30] is achieved with a truly pore- and defect-free bond, the thermal conductivity can be almost doubled. It is thus possible to increase the cooling efficiency of heat sinks, for example, even further.

It is noted that even higher thermal conductivities have been reported for other systems. For instance, with the ARB process, thermal conductivities of over 350 W/m·K could be achieved with the addition of SiC between the layers of a Cu-Al-Ni-Al-Cu sandwich [9], over 400 W/m·K for a Cu-Mg (with SiC particles) composite [8] and over 280 W/m·K for an Al-Cu functionally graded metal matrix composite by combining ARB and CRB [10]. However, in those cases the thermal conductivities were measured parallel to the layer structure and not orthogonal to the layers as was the case in the present study.

In addition to the thermal conductivity, the pores also have an impact on the mechanical properties. For instance, this was discussed by Fintová et al. [16], who showed that the largest pore in a casting is responsible for failure, not the number of pores. The decrease in fatigue life is directly related to the increase in defect size [32]. Due to the laminar gravity die casting process used in the present study, the number of pores in the bulk of the cast aluminum could be minimized compared to a more turbulent pressure die casting process [3]. In fact, the pores were found exclusively in the compound zone (cf. Figure 8). Part of these seem to be caused by the Kirkendall effect, since Bajer et al. [25] showed that substantial diffusion of silicon takes place at 450 °C and cavities form and grow due to this effect. However, pure aluminum was used here. Still, the pores were mainly observed in the compound zone close to the pure aluminum. It can therefore be assumed that diffusion of e.g., copper or gases present in the melt becomes critical during solidification due to the low cooling rate of the mold, which leads to cavities. Therefore, in addition to reducing the CZT by lowering the casting temperatures, it is important to close the resulting voids or at least keep them as small as possible, as the largest defect is responsible for the failure of the component [16]. Degassing the melt, e.g., by an inert gas introduced into the melt by means of an impeller, should reduce the amount of gas dissolved in the melt and should thus further decrease the resulting porosity. Rapid cooling of the mold below 450 °C directly after solidification of the melt could curtail diffusion and also reduce the pore size as well as the CZT.

5. Conclusions

In the present study, compound castings between copper and aluminum were produced inside an XHV-adequate atmosphere in order to enable formation of a metallurgical bond and high thermal conductivity. The results can be summarized as follows:

1. The compound zone thickness was determined based on tomography data to obtain a meaningful microstructure–thermal property–process relationship.
2. For well-bonded specimens, the thermal conductivity λ decreased as the porosity increased.
3. Thermal conductivity was largely affected by both porosity and formation of non-bonded areas at the interface. Both parameters could be tailored by adjusting the casting parameters.

4. At an apparent porosity of 4.7%, a maximum thermal conductivity of 88.3 W/m·K was realized in a specimen with a well-bonded compound zone.

Author Contributions: Conceptualization, C.K. (Christian Klose) and H.J.M.; methodology, C.K. (Christian Klose) and A.C.F.; software, C.K. (Christoph Kahra); investigation, A.C.F., A.S., and C.K. (Christoph Kahra); data curation, C.K. (Christoph Kahra); writing—original draft preparation, A.C.F.; writing—review and editing, C.K. (Christian Klose) and H.J.M.; visualization, A.C.F. and C.K. (Christoph Kahra); supervision, C.K. (Christian Klose) and H.J.M.; project administration, C.K. (Christian Klose) and H.J.M.; funding acquisition, C.K. (Christian Klose) and H.J.M. All authors have read and agreed to the published version of the manuscript.

Funding: This research was funded by the Deutsche Forschungsgemeinschaft (DFG, German Research Foundation)—Project-ID 394563137—SFB 1368.

Data Availability Statement: Data are available upon reasonable request.

Conflicts of Interest: The authors declare no conflict of interest.

References

1. Mai, T.A.; Spowage, A.C. Characterisation of dissimilar joints in laser welding of steel–kovar, copper–steel and copper–aluminium. *Mater. Sci. Eng. A* **2004**, *374*, 224–233. [CrossRef]
2. Zare, G.R.; Divandari, M.; Arabi, H. Investigation on interface of Al/Cu couples in compound casting. *Mater. Sci. Technol.* **2013**, *29*, 190–196. [CrossRef]
3. Klose, C.; Freytag, P.; Otten, M.; Thürer, S.E.; Maier, H.J. Thermal Properties of Intermetallic Phases at the Interface of Aluminum-Copper Compound Castings. *Adv. Eng. Mater.* **2018**, *20*, 1701027. [CrossRef]
4. Li, G.; Jiang, W.; Guan, F.; Zhu, J.; Yu, Y.; Fan, Z. Improving mechanical properties of AZ91D magnesium/A356 aluminum bimetal prepared by compound casting via a high velocity oxygen fuel sprayed Ni coating. *J. Magnes. Alloy.* **2022**, *10*, 1075–1085. [CrossRef]
5. Li, G.; Jiang, W.; Guan, F.; Zhu, J.; Zhang, Z.; Fan, Z. Microstructure, mechanical properties and corrosion resistance of A356 aluminum/AZ91D magnesium bimetal prepared by a compound casting combined with a novel Ni-Cu composite interlayer. *J. Mater. Process. Technol.* **2021**, *288*, 116874. [CrossRef]
6. Zhang, Z.; Jiang, W.; Li, G.; Wang, J.; Guan, F.; Jie, G.; Fan, Z. Effect of La on microstructure, mechanical properties and fracture behavior of Al/Mg bimetallic interface manufactured by compound casting. *J. Mater. Sci. Technol.* **2022**, *105*, 214–225. [CrossRef]
7. Fan, S.; Jiang, W.; Li, G.; Mo, J.; Fan, Z. Fabrication and microstructure evolution of Al/Mg bimetal using a near-net forming process. *Mater. Manuf. Process.* **2017**, *32*, 1391–1397. [CrossRef]
8. Wang, Y.; Tayyebi, M.; Tayebi, M.; Yarigarravesh, M.; Liu, S.; Zhang, H. Effect of whisker alignment on microstructure, mechanical and thermal properties of Mg-SiCw/Cu composite fabricated by a combination of casting and severe plastic deformation (SPD). *J. Magnes. Alloy.* **2022**. [CrossRef]
9. Huang, J.; Tayyebi, M.; Assari, A.H. Effect of SiC particle size and severe deformation on mechanical properties and thermal conductivity of Cu/Al/Ni/SiC composite fabricated by ARB process. *J. Manuf. Process.* **2021**, *68*, 57–68. [CrossRef]
10. Tayyebi, M.; Alizadeh, M. Thermal and wear properties of Al/Cu functionally graded metal matrix composite produced by severe plastic deformation method. *J. Manuf. Process.* **2023**, *85*, 515–526. [CrossRef]
11. Tayyebi, M.; Alizadeh, M. A novel two-step method for producing Al/Cu functionally graded metal matrix composite. *J. Alloy. Compd.* **2022**, *911*, 165078. [CrossRef]
12. Fromm, A.C.; Barienti, K.; Selmanovic, A.; Thürer, S.E.; Nürnberger, F.; Maier, H.J.; Klose, C. Oxygen-Free Compound Casting of Aluminum and Copper in a Silane-Doped Inert Gas Atmosphere: A New Approach to Increase Thermal Conductivity. *Int. J. Met.* **2022**, *20*, 1701027. [CrossRef]
13. Xu, H.; Liu, C.; Silberschmidt, V.V.; Pramana, S.S.; White, T.J.; Chen, Z.; Acoff, V.L. Behavior of aluminum oxide, intermetallics and voids in Cu–Al wire bonds. *Acta Mater.* **2011**, *59*, 5661–5673. [CrossRef]
14. Li, C.; Li, D.; Tao, X.; Chen, H.; Ouyang, Y. Molecular dynamics simulation of diffusion bonding of Al–Cu interface. *Model. Simul. Mater. Sci. Eng.* **2014**, *22*, 65013. [CrossRef]
15. Tayyebi, M.; Rahmatabadi, D.; Karimi, A.; Adhami, M.; Hashemi, R. Investigation of annealing treatment on the interfacial and mechanical properties of Al5052/Cu multilayered composites subjected to ARB process. *J. Alloys Compd.* **2021**, *871*, 159513. [CrossRef]
16. Fintová, S.; Anzelotti, G.; Konečná, R.; Nicoletto, G. Casting Pore Characterization by X-ray Computed Tomography and Metallography. *Arch. Mech. Eng.* **2010**, *57*, 263–273. [CrossRef]
17. Arnberg, L.; Mathiesen, R.H. The real-time, high-resolution x-ray video microscopy of solidification in aluminum alloys. *JOM* **2007**, *59*, 20–26. [CrossRef]
18. Yoon, J.; Kim, H.; Sim, S.-H.; Pyo, S. Characterization of Porous Cementitious Materials Using Microscopic Image Processing and X-ray CT Analysis. *Materials* **2020**, *13*, 3105. [CrossRef]

19. Nicoletto, G.; Anzelotti, G.; Konečná, R. X-ray computed tomography vs. metallography for pore sizing and fatigue of cast Al-alloys. *Procedia Eng.* **2010**, *2*, 547–554. [CrossRef]
20. Nourian-Avval, A.; Fatemi, A. Characterization and Analysis of Porosities in High Pressure Die Cast Aluminum by Using Metallography, X-Ray Radiography, and Micro-Computed Tomography. *Materials* **2020**, *13*, 3068. [CrossRef]
21. Kirkendall, E.O. Diffusion of Zinc in Alpha Brass. *Trans. AIME* **1942**, *147*, 104–110.
22. Thiry, D.; Molina-Luna, L.; Gautron, E.; Stephant, N.; Chauvin, A.; Du, K.; Ding, J.; Choi, C.-H.; Tessier, P.-Y.; El Mel, A.-A. The Kirkendall Effect in Binary Alloys: Trapping Gold in Copper Oxide Nanoshells. *Chem. Mater.* **2015**, *27*, 6374–6384. [CrossRef]
23. Yin, Y.; Rioux, R.M.; Erdonmez, C.K.; Hughes, S.; Somorjai, G.A.; Alivisatos, A.P. Formation of hollow nanocrystals through the nanoscale Kirkendall effect. *Science* **2004**, *304*, 711–714. [CrossRef] [PubMed]
24. Zeng, K.; Stierman, R.; Chiu, T.-C.; Edwards, D.; Ano, K.; Tu, K.N. Kirkendall void formation in eutectic SnPb solder joints on bare Cu and its effect on joint reliability. *J. Appl. Phys.* **2005**, *97*, 24508. [CrossRef]
25. Bajer, J.; Zaunschirm, S.; Plank, B.; Šlapáková, M.; Bajtošová, L.; Cieslar, M.; Kastner, J. Kirkendall Effect in Twin-Roll Cast AA 3003 Aluminum Alloy. *Crystals* **2022**, *12*, 607. [CrossRef]
26. Mathew, J.; Williams, M.A.; Srirangam, P. X-ray Computed Tomography Studies on Porosity Distribution in Vacuum Induction Cast Al-7Si Alloys. *JOM* **2021**, *73*, 3866–3872. [CrossRef]
27. Danielson, R.E.; Sutherland, P.L. Porosity. In *Methods of Soil Analysis*; American Society of Agronomy, Inc.: Madison, WI, USA, 1986; pp. 443–461; ISBN 9780891188643.
28. Vomocil, J.A. Porosity. In *Methods of Soil Analysis*; American Society of Agronomy, Inc.: Madison, WI, USA, 1965; pp. 299–314. ISBN 9780891182030.
29. Baehr, H.D.; Stephan, K. *Wärme- und Stoffübertragung*; Aktual. Aufl. 2016, Imprint; Springer: Berlin/Heidelberg, Germany, 2016; Volume 9, ISBN 978-3-662-49677-0.
30. Maier, H.J.; Gawlytta, R.; Fromm, A.C.; Klose, C. Increasing Thermal Conductivity in Aluminum-copper Compound Castings: Modeling and Experiments. *Submitt. J. Mater. Sci. Techn.* **2022**, 1–11. [CrossRef]
31. Mehrer, H. *Diffusion in Solids: Fundamentals, Methods, Materials, Diffusion-Controlled Processes*; Springer: Berlin/Heidelberg, Germany, 2007; ISBN 978-3-540-71488-0.
32. Wang, Q.; Apelian, D.; Lados, D. Fatigue behavior of A356-T6 aluminum cast alloys. Part I. Effect of casting defects. *J. Light Met.* **2001**, *1*, 73–84. [CrossRef]